Vietnam Journal of Science and Technology ***64***(3) (2026) 565–575
DOI: https://doi.org/10.15625/2525-2518/21773

Enhancement of photocatalytic activity of Co and Fe co-doped TiO_2 coated on modified vermiculite for removing norfloxacin antibiotic in water

Nguyen Thi Hue[1,*], Nguyen Manh Nghia[2,*], Chu Viet Hai[1], Luu Van Huyen[3], Le Quang Vinh[4], Nguyen Thi Phuong Mai[5], Ho Thanh Sang[3]

[1]*Institute of Science and Technology for Energy and Environment, Vietnam Academy of Science and Technology (VAST), 18 Hoang Quoc Viet Street, Nghia Do Ward, Ha Noi, Viet Nam*
[2]*Faculty of Physics, Hanoi National University of Education, 136 Xuan Thuy Street, Cau Giay Ward, Ha Noi, Viet Nam*
[3]*Hanoi University of Natural Resources and Environment, 41A Phu Dien Street, Phu Dien Ward, Ha Noi,Viet Nam*
[4]*Institute of Materials Science, Vietnam Academy of Science and Technology (VAST), 18 Hoang Quoc Viet Street, Nghia Do Ward, Ha Noi, Viet Nam*
[5]*Faculty of Environmental Sciences, University of Science, Viet Nam National University, 334 Nguyen Trai Street, Thanh Xuan Ward, Ha Noi, Viet Nam*

[*]Emails: *nthue2003@gmail.com*; *nghianm@hnue.edu.vn*

Received: 23 October 2024; Accepted for publication: 24 July 2025

Abstract. This study investigates the photocatalytic degradation of norfloxacin (NOR) antibiotic in water using Co and Fe co-doped TiO_2 material immobilized on modified vermiculite (VER) treated with HCl, H_2SO_4, or HNO_3. The VER treated with a 3 M HNO_3 solution exhibited a more porous surface and greater adhesion of TiO_2 crystals compared to VER treated by other acids. SEM analysis revealed uniformly spherical TiO_2 crystals with 5–10 nm size. EDS analysis confirmed the incorporation of both Fe and Co elements within the TiO_2 crystal lattice. UV-Vis spectra of the co-doped sample showed a red shift of approximately 240 nm relative to undoped TiO_2. Co-doping with Fe and Co exhibited superior photocatalytic performance compared to single-element. The photocatalytic degradation efficiency for NOR followed the order: Fe,Co_TiO_2/VER_HNO_3 > Fe,Co_TiO_2/VER_H_2SO_4 > Fe,Co_TiO_2/VER_HCl, with corresponding degradation efficiencies of 96 %, 60 %, and 46 % after 24 hours of fluorescent light illumination. The crude VER sample exhibited negligible photocatalytic activity. The Co,Fe_TiO_2/VER is easy float on the water surface, making it a promising material for water treatment applications, especially for the removal of norfloxacin antibiotics under visible light conditions.

Keywords: co-doping, TiO_2, vermiculite, norfloxacin.

Classification numbers: 2.4.2, 3.4.2, 3.6.1.

1. INTRODUCTION

Water pollution caused by pharmaceuticals has been a major concern over the past few decades. Norfloxacin (NOR) has been widely utilized in clinical, veterinary, and aquaculture applications [1–4]. The NOR has been frequently detected in lakes, municipal wastewater treatment plants, and surface waters [5, 6]. Nine antibiotics were detected, with concentrations ranging from undetectable to 2702 ng/L in lake water and approximately 449 μg/kg in lake sediment in Guangzhou, China. Among these, the NOR had the highest concentration, followed by ciprofloxacin [7]. Antibiotic concentrations have been detected in surface water in the Pudong New Area, Shanghai, China, with total concentrations of sulfonamides, quinolones, and macrolides ranging from undetectable to 14 ng/L, 30 to 344 ng/L, and undetectable to 107 ng/L. Quinolones were detected in most surface water environments and swine wastewater [8]. A study investigating antibiotic residues in treated wastewater from hospitals, wastewater from pharmaceutical manufacturing companies, and surface water in fish farming areas in Ha Noi city and Phu Tho province. The concentrations of ciprofloxacin, ofloxacin, sulfamethoxazole, and trimethoprim in treated wastewater samples were 41 μg/L, 85 μg/L, 252 μg/L, and 107 μg/L, respectively [9]. Quinolones were identified as one of three antibiotic groups present in lakes in Ha Noi city [10]. Although the quinolone group had lower concentrations than the macrolide group, several quinolone compounds were detected in lake water, including enrofloxacin (49 ng/L), ciprofloxacin (162 ng/L), ofloxacin (255 ng/L), norfloxacin (41.1 ng/L), and lomefloxacin (25.3 ng/L) [11]. Approximately 10 antibiotics from four groups have been detected in surface water. Among these, sulfonamide and quinolone were the most prevalent groups found in the Mekong Delta, Viet Nam [12].

Consequently, identifying and removing antibiotic residues from water bodies is essential. Various methods have been employed for this purpose, including adsorption [13], biodegradation, ultrasonic techniques [14], and advanced oxidation processes (AOPs) [15]. Titanium dioxide (TiO_2) is a widely used photocatalytic material due to its unique band structure and non-toxicity [16, 17]. Its capability to degrade pollutants under visible light irradiation, particularly antibiotic contaminants in water [18, 19]. The TiO_2 photocatalysis is limited by its wide bandgap and the rapid recombination of photogenerated electron-hole pairs. Metal doping (e.g., Ag, Zn) [20, 21], non-metal doping (e.g., N, S) [22, 23], and metal-nonmetal co-doping [24] have been investigated to expand the light absorption range of TiO_2. The Fe and N co-doped TiO_2 showed bandgaps of approximately 2.53 eV for the sol-gel method and 3.00 eV for the microwave method, respectively [25, 26]. The TiO_2 doped with Fe^{3+} nanoparticles has been shown to effectively remove Congo red [27]. The physical properties and composition of the TiO_2 layer formed on a carrier material are significantly influenced by the characteristics of the carrier. Vermiculite (VER), a natural mineral with a large surface area, low density, and excellent adsorption properties, showed great potential as a support material for TiO_2 due to its advantageous characteristics.

This study investigates the simultaneous doping of cobalt and iron into the crystal structure of TiO_2, along with an evaluation of its structural characteristics, morphology, and elemental composition within the TiO_2 lattice [28]. The study evaluates the efficiency of Fe, Co-doped TiO_2 in treating NOR. This research aims to evaluate the photocatalytic properties of Fe, Co-doped TiO_2 immobilized on VER, synthesized via the sol-gel method using VER treated with HNO_3, HCl, and H_2SO_4.

2. MATERIALS AND METHODS

2.1. Chemical and synthesis

Titanium tetraisopropoxide (TTIP, $C_{12}H_{28}O_4Ti$, Deajung Co., Korea), diethanolamine (DEA, Sigma – Aldrich Co. LLC) and ethanol (C_2H_5OH, 98 %, Deajung Co., Korea) were used to prepare the sol solution. Deionized water was used throughout the experiment. Nitric acid (15.5 mol, Merck Co., Germany), hydrochloric acid (18.8 mol, Merck Co., Germany), and sulfuric acid (10 mol, Merck Co., Germany) were used in the vermiculite treatment process. Natural VER clay, sourced from the Son Binh sericite mine (Viet Nam), contains SiO_2, Al_2O_3, Fe_2O_3 and MgO as its main components, with corresponding percentages of 46.2 %, 10.5 %, 9.8 % and 15.2 %. Norfloxacin ($C_{16}H_{18}FN_3O_3$, > 98 %) was obtained from Tokyo Chemical Industry (TCI), Japan. Fe^{3+} and Co^{2+} ions were prepared from $Fe(NO_3)_3{\cdot}9H_2O$ (98 %, Sigma-Aldrich) and $Co(NO_3)_2{\cdot}6H_2O$ (98 %, Sigma-Aldrich), respectively.

Natural VER was washed with deionized water, dried, crushed, and sieved through an 80-mesh wire sieve. The VER was treated with 3 M HNO_3, 3 M H_2SO_4, and 3 M HCl solutions at varying concentrations and temperatures. After being shaken, filtered, and washed with deionized water, the vermiculite was dried at 105 °C for 2 hours and then calcined at 600 °C for 4 hours.

The precursor solution of TiO_2 sol consists of a mixture of TTIP, DEA, in a molar ratio of 1:1:34. The Fe^{3+} and Co^{2+} co-doped TiO_2 sol was prepared by adding $Fe(NO_3)_3{\cdot}9H_2O$ and $Co(NO_3)_2{\cdot}6H_2O$ to the sol solution, with molar ratios of Fe^{3+}/Ti^{4+} and Co^{2+}/Ti^{4+} both set at 6 %. Denatured 2 grams VER was soaked in the Fe, Co co-doped TiO_2 solution for 60 minutes, dried at room temperature for one day, and then annealed at 500 °C for 3 hours. The soaking, drying, and annealing steps were repeated three times to obtain pure Fe, Co co-doped TiO_2 immobilized on VER. After modification with different acids (HNO_3, H_2SO_4, HCl) and immobilization with TiO_2, are denoted as TiO_2/VER_HNO_3, TiO_2/VER_H_2SO_4, and TiO_2/VER_HCl.

VER samples soaked in HNO_3, H_2SO_4, and HCl acids at a concentration of 3 M are denoted as VER_HNO_3 3 M, VER_H_2SO_4 3 M and VER_HCl 3 M, respectively. The VER is also denoted according to the soaking time in different acid solutions; for example, the VER soaked in HNO_3 for 12 hours is denoted as TiO_2/VER_HNO_3_12 h, similarly for TiO_2/VER_HNO_3_24 h and TiO_2/VER_H_2SO_4_24 h, ect. The samples co-doped with Fe,Co into TiO_2 impregnated on acidified VER are denoted as Fe,Co_TiO_2/VER_HNO_3, Fe,Co_TiO_2/VER_H_2SO_4, and Fe,Co_TiO_2/VER_HCl. Samples denoted as Fe,Co_TiO_2/VER 2 %; Fe,Co_TiO_2/VER 4 %; and Fe,Co_TiO_2/VER 6 % mean that the molar numbers of Fe and Co added to the Fe,Co_TiO_2/VER sample are 2 %, 4 %, and 6%, respectively.

2.2. Characterization

The crystal structures of the samples were characterized by an X-ray diffractometer (D8-ADVANCE). Surface morphology and microstructure were measured by scanning electron microscopy (SEM, S-4800, Hitachi, Japan). The elemental compositions and electronic states were determined via X-ray photoelectron spectroscopy (EDS, Tecnai Osiris 200kV, FEI, USA). The band gap was obtained from the ultraviolet - visible (UV - vis) absorption spectra measured using a V670 system (Jasco, USA). The Zeta potential was measured using a PMT detectorphoto multiplier (Horiba, Japan, SZ-100-Z2). The porosity properties were determined by using a 3Flex surface characterization analyzer (Micromeritics, USA). Norfloxacin concentration was determined by HPLC, Shimadzu, Japan.

2.3. Photocatalytic activity test

The photocatalytic set up based on a fixed bed reactor is schematically summarized in Figure 1. Two grams of the sample were placed in a quartz tube,with a diameter of 1 cm and a length of 20 cm. This tube was illuminated from 5 cm above a visible light source (18 W T8 Philips Daylight/865 600 nm lamp). Two liters of a solution with an initial NOR concentration of 10 ppm were held in a reservoir and circulated through the photocatalytic system by a diaphragm water pump. The flow rate was set to 1 mL/min. 1 mL samples in the reservoir were collected into vials at regular intervals.

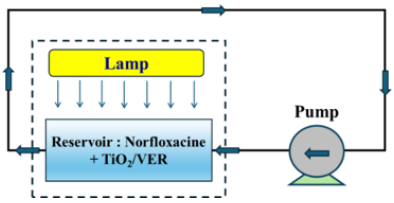

Figure 1. Schematic diagram of the photocatalytic device for Norfloxacine degradation.

3. RESULTS AND DISCUSSION

3.1. XRD analysis

The XRD patterns of TiO_2/VER samples are illustrated in Figures 2 and 3. For the TiO_2/VER samples, a significant diffraction peak at 25.4° can be clearly observed, which is indexed to the (101) plane of TiO_2 anatase. After treating VER carrier with H_2SO_4, HCl, or HNO_3 acid, the peak positions remained unchanged, but the intensity of the TiO_2 anatase peaks increased compared to the corresponding peaks observed from the untreated samples. Additionally, the diffraction peak at 25.4° of the HNO_3-treated VER was slightly narrower than that of the samples treated with other acids, suggesting that this acid might be suitable for preparing VER carrier.

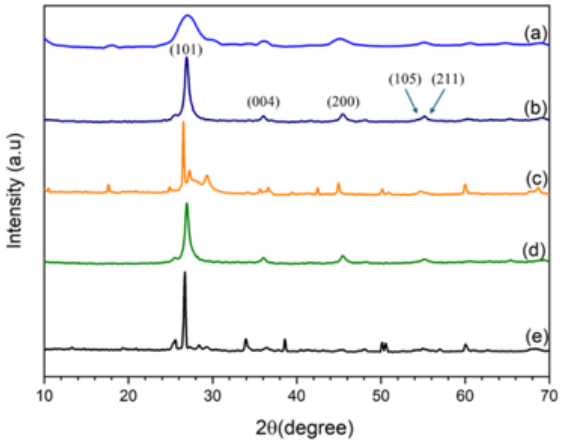

Figure 2. XRD pattern of the samples: (a) raw VER before denaturation, (b) TiO_2/VER, (c) TiO_2/VER_HCl 3 M, (d) TiO_2/VER_H_2SO_4 3 M, and (e) TiO_2/VER_HNO_3 3 M.

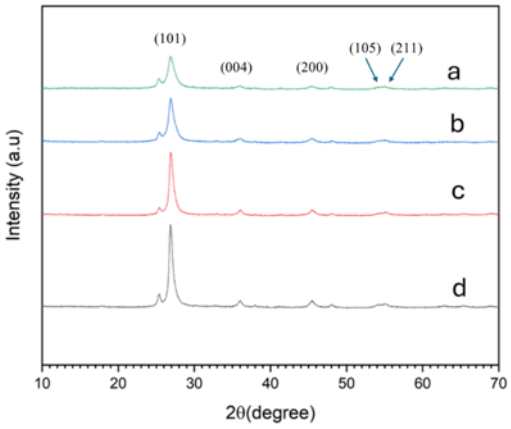

Figure 3. XRD pattern of the samples: (a) TiO_2/VER, (b) Fe,Co_TiO_2/VER 2 %, (c) Fe,Co_TiO_2/VER 4 %, and (d) Fe,Co_TiO_2/VER 6 %.

In the XRD pattern of Fe,Co_TiO_2/VER samples, no peaks corresponding to crystalline iron or cobalt oxides were observed. This result agrees with our previous findings on single-element doping [24]. Therefore, it is possible that Fe and Co were successfully incorporated into the TiO_2 lattice.

3.2. SEM examination

Figure 4 displays SEM images of VER treated with HNO_3, H_2SO_4, and HCl. In Figure 5a, the surface of the untreated VER exhibits a multilayered, sandwich-like structure, with lamellae stacked on top of each other resembling a deck of cards. After acid treatment (Figures 4b–d), the VER surface exhibited signs of significant cracking, peeling, and an increase in roughness. These modifications enhance the potential of VER as a support material, as the increased porosity of the surface allows TiO_2 to adhere more effectively.

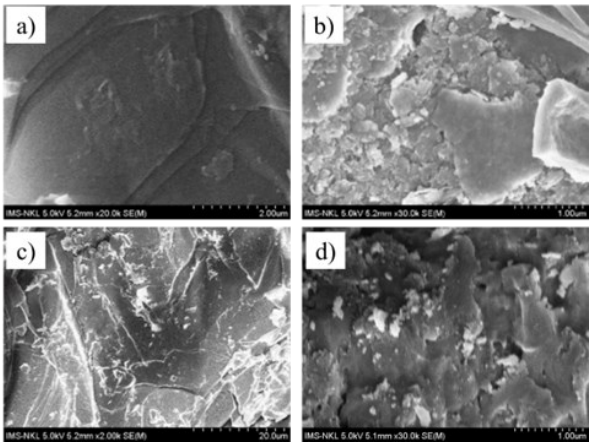

Figure 4. SEM images of VER (a), VER_HNO_3 3 M (b), VER_H_2SO_4 3 M (c), and VER_HCl 3 M (d) samples.

Figure 5 displays SEM images of VER treated with varying durations of acid immersion. In Figures 5a-c, the results indicated that the VER surface became increasingly fractured and porous. The adhesion and coating density of TiO_2 on the VER surface varied significantly with the duration of acid immersion. Compared to other durations, the VER surface displayed increased cracking when immersed in acid for more than 12 hours. However, the samples immersed for 24 and 36 hours exhibited a more uniform surface. Therefore, soaking VER for 24 hours proved sufficient to activate the surface for TiO_2 coating. Figures 5b, d, and e show SEM images of the TiO_2/VER samples immersed for 24 hours in 3 M HNO_3, 3 M H_2SO_4, and 3 M HCl solutions. The VER sample immersed in HNO_3 exhibited more uniform porosity and cracking compared to the samples treated with other acids. The TiO_2 crystals adhered more uniformly and densely to the VER surface when the material was soaked in HNO_3. These results suggest that VER, when soaked for 24 hours in HNO_3, serves as an effective carrier material for the attachment of TiO_2 crystals.

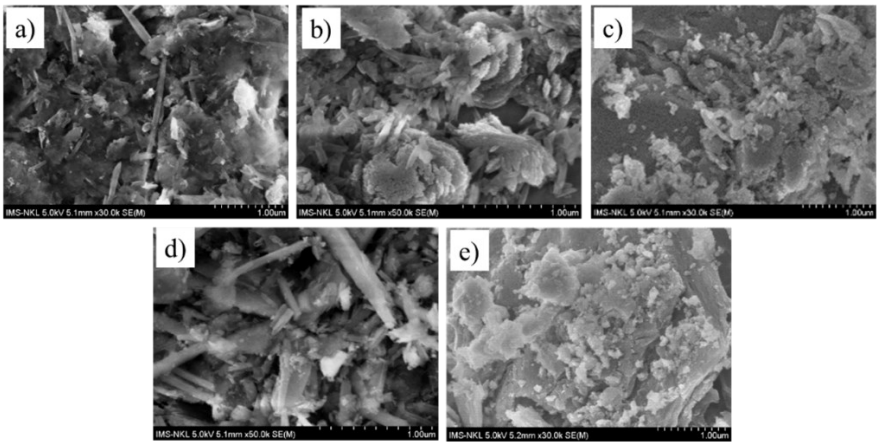

Figure 5. SEM images of TiO_2/VER_HNO_3_12 h (a), TiO_2/VER_HNO_3_24 h (b), TiO_2/VER_HNO_3_36 h (c), TiO_2/VER_H_2SO_4_24 h (d), and TiO_2/VER_HCl_24 h (e) samples.

Figure 6 demonstrates SEM and EDS spectra of the Fe,Co co-doped TiO_2/VER sample. Following acid treatment, the VER became an ideal substrate material for TiO_2, with its surface exhibiting small, round particles measuring 5–10 nm in grain size, uniformly distributed across the vermiculite. Occasionally, a few rod-shaped crystals, measuring 10 × 10 × 50 to 500 nm, were observed. This enhanced the contact between the catalytic material and the environment. The chemical composition of the Fe,Co_TiO_2/VER sample was analyzed using energy-dispersive X-ray spectroscopy (EDS), as illustrated in Figure 8c and summarized in Table 1. The results confirmed the presence of TiO_2 in the material. With an equal molar ratio of Fe and Co added, the EDS analysis revealed a stronger Fe ion peak intensity, likely due to the magnetic properties of Fe, which lead to stronger interactions between Fe^{3+} and Ti^{4+} ions.

Table 1. Chemical composition of the Fe,Co_TiO_2/VER sample analyzed by EDS technique.

Element	O	Mg	Al	Si	K	Ti	Fe	Co	Ca	Total
Weight %	5.44	5.08	4.58	14.92	3.89	10.66	13.91	0.64	0.87	100
Atomic %	65.23	4.8	3.9	12.2	2.28	5.11	5.72	0.25	0.5	100

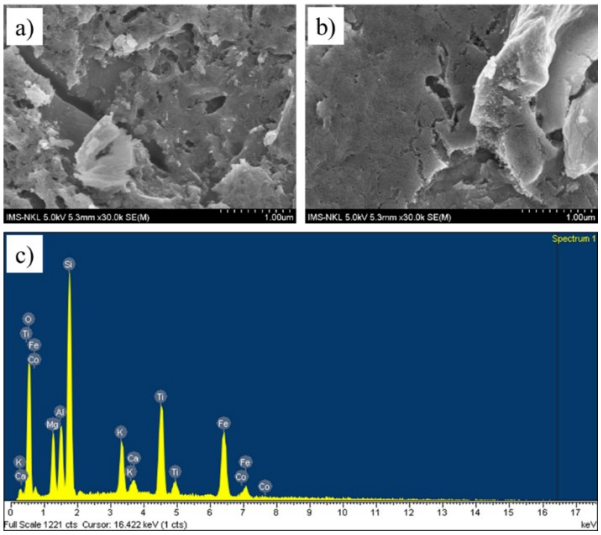

Figure 6. SEM images of TiO_2/VER (a), Fe,Co_TiO_2/VER (b), and EDS spectra of Fe,Co_TiO_2/VER (c) samples.

3.3. Porosity

Figure 7 shows the nitrogen adsorption-desorption isotherms of the TiO_2/VER samples. All adsorption-desorption isotherms of TiO_2/VER are classified as type IV, according to the IUPAC classification. The results clearly demonstrated that the specific surface area of TiO_2/VER increased significantly following the acid treatment process. Furthermore, the Fe,Co_TiO_2/VER activated with HNO_3 exhibited the largest specific surface area, which was 2.2 times greater than that of VER activated with H_2SO_4 and 3.8 times greater than that of VER activated with HCl. Porous frameworks may form when strong HNO_3 acid removes aluminum or silica compounds. Thus, these mesopores account for the sharp increase in N_2 adsorption at high pressure, which is attributed to the capillary effect. Consequently, vermiculite treated with HNO_3 proves to be an excellent catalyst carrier, owing to its large specific surface area.

Zeta potential measurements were performed to evaluate the stability of the TiO_2/VER composite in solution. The zeta potential values for TiO_2/VER_HNO_3, TiO_2/VER_H_2SO_4, and TiO_2/VER_HCl are presented in Table 2. The TiO_2/VER_HNO_3 sample exhibited the most negative zeta potential, reflecting the strongest electrostatic repulsion between TiO_2 particles and the solution. This resulted in enhanced dispersion stability.

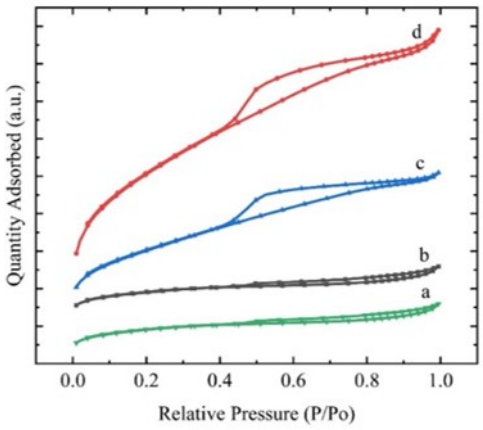

Figure 7. N_2 adsorption-desorption isotherms of VER (a), Fe,Co_TiO_2/VER (b), Fe,Co_TiO_2/VER_H_2SO_4 (c), and Fe,Co_TiO_2/VER_HNO_3 (d) samples.

Table 2. Surface area (S), pore volume (V), average pore diameter (d), Zeta potential U_P, and Zeta deviation (U_D) of TiO_2/VER modified in acid solutions.

Sample	S (m^2/g)	V (cm^3/g)	d (Å)	U_P (mV)	U_D (mV)
Raw VER	60	0.049	32.9		
Fe,Co_TiO_2/VER_HCl	94	0.079	33.7	-24.1	45.6
Fe,Co_TiO_2/VER_H_2SO_4	161	0.134	33.2	-25.2	49.8
Fe,Co_TiO_2/VER_HNO_3	351	0.275	31.3	-34.8	8.28

3.4. Light absorption

Figure 8 shows the optical absorbance of TiO_2/VER, Fe_TiO_2/VER, Co_TiO_2/VER, and Fe,Co_TiO_2/VER samples. The red shift of absorption edges was more obvious for the Fe,Co_TiO_2/VER sample, moving from 506 nm to 744 nm. The bandgap energy of the samples was estimated using Tauc's method by fitting the absorption equation $(\alpha h\upsilon)^n = A(h\upsilon - E_g)$, where α is the absorbance, hν is the photon energy, and n is the factor depending on the nature of the electron transition. The E_g values were estimated by extrapolating the linear region of the $(\alpha h\nu)^n$ vs. (hν) plot and determining the x-axis intersection point. Anatase TiO_2 exhibits indirectly allowed transitions corresponding to n = 1/2. However, Tauc plot analysis using n = 1/2 yielded bandgap energies in the near-infrared region (E_g < 1.6 eV) for all our samples, which is inconsistent with the observed absorption edge. Moreover, when the TiO_2 is supported on vermiculite, our experimental data indicate that the n = 2 transition yields the highest precision in the Tauc plot analysis [29]. In Figure 8, the estimated optical bandgaps for TiO_2/VER, Fe_TiO_2/VER, Co_TiO_2/VER, and Fe,Co_TiO_2/VER are 2.1 eV, 2.4 eV, 2.6 eV, and 2.8 eV, respectively. The decrease in the bandgap energy Eg of the TiO_2/VER photocatalyst is likely due to the synergistic influence of the negative layer charge present in vermiculite. Vermiculite

reduces the bandgap of TiO_2 by introducing new energy states via interlayer ions, surface groups, or material interactions, useful for photocatalysis and electronics [30,31].

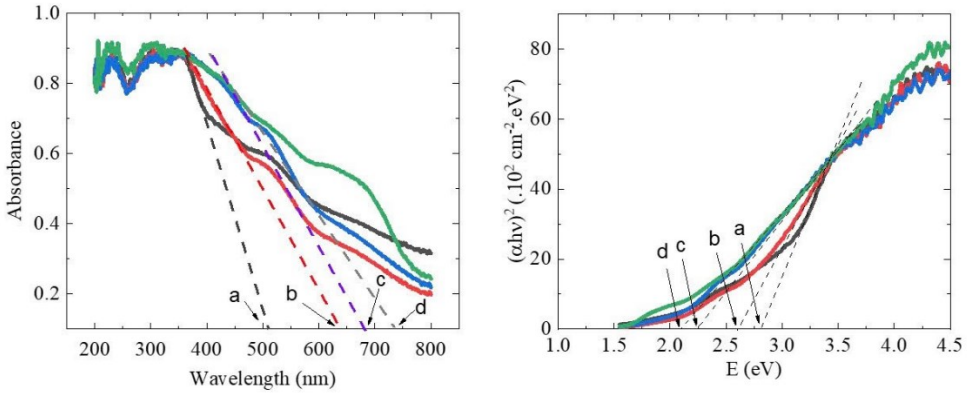

Figure 8. UV-vis spectra (left) and Tauc's plot (right) of TiO_2/VER (a), Fe_TiO_2/VER (b), Co_TiO_2/VER (c), and Fe,Co_TiO_2/VER (d) samples.

The introduction of Fe and Co dopants led to a red shift in the absorption edge observed in the UV-vis spectra. This is attributed to the overlapping conduction bands between the Ti^{+4} ions of TiO_2 and the 3d electrons of Fe^{+3} ions and 2d electrons of Co^{2+} ions, resulting in a shift in wavelength towards longer wavelengths. On the other hand, the absorption of electrons from the defect state always leads to light absorption, the intensity of the band tailing can directly reflect the number of defect states. It can be seen that the Fe,Co_TiO_2/VER has more defect states.

3.5. Photocatalytic activities

Raw VER and the co-doped samples (Fe,Co_TiO_2) coated on VER modified with HCl, H_2SO_4, and HNO_3 were tested for their norfloxacin (NOR) treatment ability. Figure 9 shows that, under dark conditions, all four samples (raw VER; Fe,Co_TiO_2/VER_HCl; Fe,Co_TiO_2/VER_H_2SO_4; Fe,Co_TiO_2/VER_HNO_3) achieved maximum NOR adsorption within 12 hours, with NOR concentration decreasing by approximately 2 ppm compared to the initial concentration. Immediately afterward, fluorescent illumination experiments were conducted to assess the photocatalytic oxidation efficiency over the next 24 hours. For the raw VER sample, the NOR concentration showed the smallest decrease compared to the other three samples. The rate of NOR concentration reduction varied among the samples, with the Fe,Co_TiO_2/VER_HNO_3 sample exhibiting the highest decrease. The photocatalytic degradation efficiency followed the order: (Fe,Co)_TiO_2/VER_HNO_3 > (Fe,Co)_TiO_2/VER_H_2SO_4 > (Fe,Co)_TiO_2/VER_HCl, with corresponding residual NOR concentrations of approximately 0.3

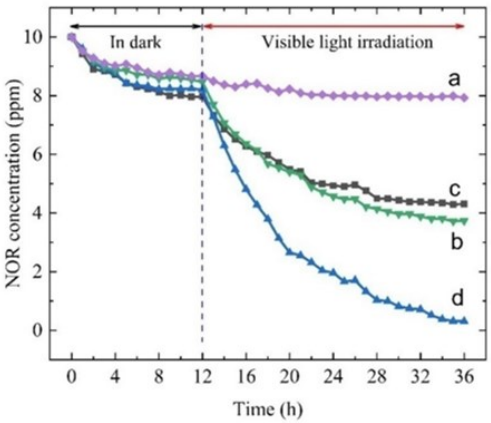

Figure 9. Photocatalytic degradation efficiency of norfloxacin using raw VER (a), Fe,Co_TiO_2/VER_HCl (b), Fe,Co_TiO_2/VER_H_2SO_4 (c), and Fe,Co_TiO_2/VER_HNO_3 (d) samples.

ppm, 4.3 ppm, and 5 ppm, respectively. The raw VER sample showed no photocatalytic activity under illuminated conditions, with a slight decrease in the NOR concentration after 24 hours of exposure to light.

The photocatalytic degradation efficiency follows the order: (Fe,Co)_TiO_2/VER_HNO_3 > (Fe,Co)_TiO_2/VER_H_2SO_4 > (Fe,Co)_TiO_2/VER_HCl > raw VER, with coresponding degradation efficiencies of 96 %, 60 %, 46 %, and 15 %. The raw VER sample demonstrated negligible photocatalytic activity, showing only a slight decrease in NOR concentration after 24 hours of illumination. This aligns with the red shift observed in the adsorption spectra, which suggests enhanced light absorption performance

4. CONCLUSIONS

TiO_2 was synthesized on vermiculite using the sol-gel method. The TiO_2 coating was applied to VER treated with 3 M HNO_3, 3 M H_2SO_4, and 3 M HCl solutions. Fe and Co were co-doped into TiO_2 at an optimal molar ratio of Fe and Co relative to Ti^{4+}, where each element accounted for 6 %. EDS analysis verified the uniform distribution of Ti, Fe, and Co elements across the VER surface. Co-doping broadened the light absorption range of TiO_2, shifting it toward longer wavelengths. The as-synthesized Fe,Co co-doped TiO_2 immobilized on VER demonstrated superior photodegradation rates of NOR under fluorescent light irradiation. This performance can be attributed to its small nanoparticle size and large surface area. Among the various acid treatments, VER modified with 3 M HNO_3 exhibited the highest NOR degradation efficiency, outperforming Fe,Co_TiO_2/VER_H_2SO_4, Fe,Co_TiO_2/VER_HCl, and raw VER. These results demonstrate the enhanced photocatalytic activity of the Fe,Co_TiO_2/VER composite for antibiotic degradation in water under visible light sources.

Acknowledgements. This research was supported by a grant from the Senior Researchers Project (NVCC 31.02/24-25). The authors would like to acknowledge the support and guidance provided by the leadership board of the Vietnam Academy of Science and Technology.

CRediT authorship contribution statement. Nguyen Thi Hue: Investigation, Supervision, Writing - review & editing, Funding acquisition. Nguyen Manh Nghia: Investigation, Writing - original draft. Chu Viet Hai: Formal analysis, Writing - review & editing. Luu Van Huyen, Le Quang Vinh: Investigation. Nguyen Thi Phuong Mai: Formal analysis. Ho Thanh Sang: Investigation.

Declaration of competing interest. The authors declare that there is no conflict of interest between them.

REFERENCES

1. Huerta-Fontela M., Galceran M. T., Ventura F. – Occurrence and removal of pharmaceuticals and hormones through drinking water treatment. Water Res., **45** (2011) 1432–1442. https://doi.org/10.1016/j.watres.2010.10.036.
2. Mons M. N., Hoogenboom A. C., Noi T. H. M. – Pharmaceuticals and drinking water supply in the Netherlands, KIWA Water Research, Nieuwegein (2003).
3. Huang Y.-H., Liu Y., Du P.-P., Zeng L.-J., Mo C.-H., Li Y.-W., Lü H., Cai Q.-Y. – Occurrence and distribution of antibiotics and antibiotic resistant genes in water and sediments of urban rivers with black-odor water in Guangzhou, South China. Sci. Total Environ., **670** (2019) 170–180. https://doi.org/10.1016/j.scitotenv.2019.03.168.
4. Ebele A. J., Oluseyi T., Drage D. S., Harrad S., Abou-Elwafa Abdallah M. – Occurrence, seasonal variation and human exposure to pharmaceuticals and personal care products in surface water,

groundwater and drinking water in Lagos State, Nigeria. Emerg. Contam., **6** (2020) 124–132. https://doi.org/10.1016/j.emcon.2020.02.004.
5. Luo Y., Xu L., Rysz M., Wang Y., Zhang H., Alvarez P. J. J. – Occurrence and transport of tetracycline, sulfonamide, quinolone, and macrolide antibiotics in the Haihe River Basin, China. Environ. Sci. Technol., **45** (2011) 1827–1833. https://doi.org/10.1021/es104009s.
6. Pan C., Bao Y., Xu B. – Seasonal variation of antibiotics in surface water of Pudong New Area of Shanghai, China and the occurrence in typical wastewater sources. Chemosphere, **239** (2020) 124816. https://doi.org/10.1016/j.chemosphere.2019.124816.
7. Huang Y.-H., Liu Y., Du P.-P., Zeng L.-J., Mo C.-H., Li Y.-W., Lü H., Cai Q.-Y. – Occurrence and distribution of antibiotics and antibiotic resistant genes in water and sediments of urban rivers with black-odor water in Guangzhou, South China. Sci. Total Environ., **670** (2019) 170–180. https://doi.org/10.1016/j.scitotenv.2019.03.168.
8. Pan C., Bao Y., Xu B. – Seasonal variation of antibiotics in surface water of Pudong New Area of Shanghai, China and the occurrence in typical wastewater sources. Chemosphere, **239** (2020) 124816. https://doi.org/10.1016/j.chemosphere.2019.124816.
9. Thai P. K., Ky L. X., Binh V. N., Nhung P. H., Nhan P. T., Hieu N. Q., Dang N. T. T., Tam N. K. B., Anh N. T. K. – Occurrence of antibiotic residues and antibiotic-resistant bacteria in effluents of pharmaceutical manufacturers and other sources around Hanoi, Vietnam. Sci. Total Environ., **645** (2018) 393–400. https://doi.org/10.1016/j.scitotenv.2018.07.126.
10. Pham T. T. Y. – Thesis on research and evaluation of residues of some antibiotics in water and aquatic animals in some lakes in Hanoi. PhD Thesis, Hanoi University of Science and Technology (2017).
11. Takasu H., Suzuki S., Reungsang A., Viet P. H. – Fluoroquinolone (FQ) contamination does not correlate with occurrence of FQ-resistant bacteria in aquatic environments of Vietnam and Thailand. Microbes Environ., **26** (2011) 135–143. https://doi.org/10.1264/jsme2.me10204.
12. Nguyen Dang Giang C., Sebesvari Z., Renaud F., Rosendahl I., Hoang Minh Q., Amelung W. – Occurrence and dissipation of the antibiotics sulfamethoxazole, sulfadiazine, trimethoprim, and enrofloxacin in the Mekong Delta, Vietnam. PLoS One, **10** (2015) e0131855. https://doi.org/10.1371/journal.pone.0131855.
13. Ahmed M. B., Zhou J. L., Ngo H. H., Guo W. – Adsorptive removal of antibiotics from water and wastewater: Progress and challenges. Sci. Total Environ., **532** (2015) 112–126. https://doi.org/10.1016/j.scitotenv.2015.05.130.
14. Malato S., Blanco J., Vidal A., Fernández P., Cáceres J., Trincado P., Oliveira J. C., Vincent M. – New large solar photocatalytic plant: Set-up and preliminary results. Chemosphere, **47** (2002) 235–240. https://doi.org/10.1016/S0045-6535(01)00220-X.
15. Glaze W. H. – Drinking-water treatment with ozone. Environ. Sci. Technol., **21** (1987) 224–230. https://doi.org/10.1021/es00157a001.
16. Varshney G., Kanel S. R., Kempisty D. M., Varshney V., Agrawal A., Sahle-Demessie E., Varma R. S., Nadagouda M. N. – Nanoscale TiO_2 films and their application in remediation of organic pollutants. Coord. Chem. Rev., **306** (2016) 43–64. https://doi.org/10.1016/j.ccr.2015.06.011.
17. Fakhouri H., Arefi-Khonsari F., Jaiswal A., Pulpytel J. – Enhanced visible light photoactivity and charge separation in TiO_2/TiN bilayer thin films. Appl. Catal. A, **492** (2015) 83–92. https://doi.org/10.1016/j.apcata.2014.12.030.
18. Wei Z., Liu J., Shangguan W. – A review on photocatalysis in antibiotic wastewater: Pollutant degradation and hydrogen production. Chin. J. Catal., **41** (2020) 1440–1450. https://doi.org/10.1016/s1872-2067(19)63448-0.
19. Homem V., Santos L. – Degradation and removal methods of antibiotics from aqueous matrices — A review. J. Environ. Manage., **92** (2011) 2304–2347. https://doi.org/10.1016/j.jenvman.2011.05.023.
20. Ali F., Moin-ud-Din G., Iqbal M., Nazir A., Altaf I., Alwadai N., Siddiqua U. H., Younas U., Ali A., Kausar A., et al. – Ag and Zn doped TiO_2 nano-catalyst synthesis via a facile green route and their catalytic activity for the remediation of dyes. J. Mater. Res. Technol., **23** (2023) 3626–3637. https://doi.org/10.1016/j.jmrt.2023.02.011.

21. Nguyen K. N., Nguyen T. T. M. – Synthesis of silver-doped TiO_2 nanoparticles with highly efficient adsorption of Congo red. Vietnam J. Chem., **62** (2024) 827–837. https://doi.org/10.1002/vjch.202400039.
22. Fakhouri H., Pulpytel J., Smith W., Zolfaghari A., Mortaheb H. R., Meshkini F., Jafari R., Sutter E., Arefi-Khonsari F. – Control of the visible and UV light water splitting and photocatalysis of nitrogen doped TiO_2 thin films deposited by reactive magnetron sputtering. Appl. Catal. B, **144** (2014) 12–21. https://doi.org/10.1016/j.apcatb.2013.06.028.
23. Nguyen L. T., Nguyen H. T., Pham T.-D., Tran T. D., Chu H. T., Dang H. T., Nguyen V.-H., Nguyen K. M., Pham T. T., Van der Bruggen B. – Visible light driven photocatalytic degradation of ciprofloxacin by N, S co-doped TiO_2: The effect of operational parameters. Top. Catal., **63** (2020) 985–995. https://doi.org/10.1007/s11244-020-01319-7.
24. Li T., Abdelhaleem A., Chu W., Pu S., Qi F., Zou J. – S-doped TiO_2 photocatalyst for visible LED mediated oxone activation: Kinetics and mechanism study for the photocatalytic degradation of pyrimethanil fungicide. Chem. Eng. J., **411** (2021) 128450. https://doi.org/10.1016/j.cej.2021.128450.
25. El Mragui A., Aadnan I., Zegaoui O., Esteves da Silva J. C. G. – Physico-chemical characterization and photocatalytic activity assessment under UV-A and visible-light irradiation of iron-doped TiO_2 nanoparticles. Arab. J. Chem., **16** (2023) 105331. https://doi.org/10.1016/j.arabjc.2023.105331.
26. Nguyen N. M., Nguyen H. T., Negishi N., Nguyen K. C., Luc H. H., Duong V. Q. – Effects of Ni doping and silica gel bead support on characteristics of TiO_2 catalyst. J. Electron. Mater., **51** (2022) 6204–6212. https://doi.org/10.1007/s11664-022-09867-2.
27. Nga N. K., Nga N. T. T. – Highly adsorptive removal of Congo red from aqueous solution using TiO_2 doped with Fe^{3+} nanoparticles. Colloid Polym. Sci., **301** (2023) 491–503. https://doi.org/10.1007/s00396-023-05084-3.
28. Mai N. T. T., Nga N. K., Hue D. T. M., Dung T. N., Chinh H. D., Huy T. Q. – Characterization of Co^{2+} and Fe^{3+} codoped TiO_2 nanomaterials for photocatalytic degradation of organic pollutants under visible light irradiation. Adsorpt. Sci. Technol., **2021** (2021) 9193052. https://doi.org/10.1155/2021/9193052.
29. Chkirida S., Zari N., Achour R., Qaiss A. el kacem, Bouhfid R. – Effect of iron doped titanium oxide encapsulated in alginate on photocatalytic activity for the removal of dye pollutants. RSC Adv., **10** (2020) 22311–22317. https://doi.org/10.1039/d0ra02898c.
30. Valášková M., Kočí K., Madejová J., Matějová L., Pavlovský J., Barrocas B. T., Klemencová K. – α-Fe_2O_3 nanoparticles/iron-containing vermiculite composites: Structural, textural, optical and photocatalytic properties. Minerals, **12** (2022) 607. https://doi.org/10.3390/min12050607.
31. Penaloza D. P. Jr. – Modified clay for the synthesis of clay-based nanocomposites. Epitoanyag-J. Silic. Based Compos. Mater., **71** (2019) 5–11. https://doi.org/10.14382/epitoanyag-jsbcm.2019.2.